DOPPLER-SHIFTED ION WAVES UPSTREAM OF THE EARTH'S
BOWSHOCK

by

Stephen A. Fuselier

A thesis submitted in partial fulfillment of the

requirements of the Master of Science degree in

Physics in the Graduate College of

The University of Iowa

1983

Thesis supervisor: Professor Donald A. Gurnett

Graduate College
The University of Iowa
Iowa City, Iowa

CERTIFICATE OF APPROVAL

———————————————

MASTER'S THESIS

———————————

This is to certify that the Master's thesis of

Stephen A. Fuselier

has been approved by the Examining Committee
for the thesis requirement for the Master of
Science degree in Physics at the May, 1983
graduation.

Thesis committee: _____
                  Thesis supervisor

                  _____
                  Member

                  _____
                  Member

ACKNOWLEDGEMENTS

Other people outside the department that helped were Bill Feldman who provided important data on the solar wind and C. Russell who provided magnetic field data. Dr. Dennis Gallagher's work on short wavelength electrostatic waves in the magnetosheath provided the basis for this study. I would like to especially thank my wife, Bette for her support these past two years. She continues to be the most important person I can share my problems and enthusiasm with.

ABSTRACT

The identification and explanation of short wavelength antenna interference effects observed in spacecraft plasma wave data have provided an important new method of determining limits on the wavelength, direction of propagation, and Doppler shift of short wavelength electrostatic waves. Using the ISEE-1 wideband electric field data, short wavelength interference effects have been identified in the ion waves upstream of Earth's bowshock. This identification implies that wavelengths of the upstream ion waves are shorter than the antenna length. The study of the antenna interference effects has also provided new measurements of the direction of propagation of the ion waves. The new measurements show that the wave vectors of the ion waves are not parallel to the interplanetary magnetic field (IMF) as previously reported. Indications show that the waves propagate at an average angle of 40 degrees to the IMF. In addition, analysis of the Doppler shift of the short wavelength ion waves has provided a measure, ment of of the dispersion relation, $\omega_0(k)$. The upper limit on the rest frame frequency was found to be on the order of the ion plasma frequency. At this frequency, the wavelength is on the order of a few times the Debye length. The results of the study of the interference effects are used to identify the ion waves in the upstream region as Doppler-shifted ion acoustic waves.

TABLE OF CONTENTS

LIST OF TABLES

LIST OF FIGURES

I. INTRODUCTION

Electrostatic waves in the region upstream of Earth's bowshock with frequencies ranging from 0 to 10 kHz were first identified by Scarf et al. [1970]. Scarf et al. reported that the electrostatic waves were associated with energetic ion beams produced in the bowshock. Gurnett and Frank [1978], using wave data from the IMP 6 spacecraft, made the first measurements of the wavelength of the upstream electrostatic waves. These measurements gave the first indication that the electrostatic waves had wavelengths on the order of a few times the Debye length. Based on the short wavelengths and other characteristics similar to the ion acoustic waves observed in the solar wind, Gurnett and Frank concluded that the upstream electrostatic waves were ion acoustic waves Doppler-shifted from below the ion plasma frequency to frequencies of 1 to 10 kHz by the motion of the solar wind. The term "ion waves" was used by Rodriguez [1981], who questioned the short wavelength characteristic and suggested, but could not demonstrate, that a Buneman-like instability was responsible for producing the waves. Gary [1978 and 1981] suggested that ion waves in the upstream region be called ion acoustic-like waves because in his theory the waves were generated by an ion beam mode which is technically different from the ion acoustic mode. Lemons et al. [1979] considered both a beam-plasma interaction and an ion-electron drift instability but could

not demonstrate an instability that would generate field aligned ion
acoustic waves using typical upstream plasma parameters. Because of
the difficulty in identifying the instability that can produce upstream
ion waves, other instabilities such as the ion density gradient insta-
bility [Wu et al., 1982] have been suggested. However, the exact
mechanism for producing upstream ion waves remains unknown.

A more recent observational study of the ion waves has been done
by Anderson et al. [1981] using data from the ISEE-1 and -2 spacecraft.
By analyzing plasma wave electric field data, Anderson et al. found
that the wavelength of the ion waves in the upstream region was between
30 and 215 meters and the direction of propagation was primarily paral-
lel to the ambient magnetic field. Using wave and particle data,
Anderson et al. verified that ion waves in the upstream region are
associated with reflected ion flux enhancements. Based on these obser-
vations, it was concluded by Anderson et al., in agreement with Gurnett
and Frank [1978], that the ion waves observed were ion acoustic waves
Doppler shifted into the 1 to 10 kHz frequency range by the solar wind.

Measurements of the propagation direction made by Anderson et al.
were difficult to make due to rapid fluctuations in the frequency and
intensity of the ion waves. In addition, the Doppler shift character-
istic of the waves could only be suggested on the basis that ion waves
in the upstream region are rarely observed above 11 kHz. This cutoff
frequency of 11 kHz is the maximum allowable Doppler shift, assuming
that the wavelength cannot be less than 2π times the Debye length
[Anderson et al., 1981].

The purpose of this work is to repeat the determination of wave-length and propagation direction of the ion waves using an independent and much more powerful method. In addition, the Doppler shift of the ion waves is determined and a measurement of the rest frame frequency as a function of the magnitude of the wave vector is obtained.

The wideband wave data used in this study came from the wideband receivers in the University of Iowa Plasma wave experiment on ISEE-1 and -2. More detailed information on the plasma wave instruments can be found in Gurnett et al. [1978]. Both spacecraft have essentially identical wideband receivers. The primary difference in the two instruments is the electric antenna. The electric dipole antenna on ISEE-1 has a tip-to-tip length of 215 meters, whereas on ISEE-2 the tip-to-tip length is 30 meters.

The method of determination of the wavelength, direction of propagation, and Doppler shift involves the study of spin modulated antenna interference patterns in the wideband data from ISEE-1. These interference patterns were first identified by Anderson et al. [1982] in wideband data from the outer magnetosheath, where waves very similar to the ion waves upstream are observed. The interference patterns have a characteristic shape first described by Anderson et al. as "festoon-shaped" emissions. Gallagher [1982] explained the interference patterns as being due to spin modulated interference effects that occur when the electrostatic waves have wavelengths shorter than the antenna length.

In this work, spin modulated interference patterns are identifed in wideband frequency-time spectrograms from the region upstream of the

bowshock. An example of the interference pattern observed is presented in Figure 1. The upper panel in Figure 1 shows the characteristic shape of the electric field emissions. The lower panel in Figure 1 is a frequency-time spectrogram from the ISEE-1 wideband receiver for December 24, 1977. ISEE-1 at this time was located in the upstream region at a distance of about 22 R_E and a magnetic local time of about 6.1 hours. The periodic change in frequency in the lower panel of Figure 1 from 17^h 23^m 48^s to 17^h 23^m 50^s occurs at one-half the space-craft rotation period. As will be shown, this periodic change in frequency can be used to determine the direction of the wave vector projected into the spacecraft spin plane. The direction obtained is then compared to the magnetic field direction projected into the spin plane.

In addition, the nulls in intensity observed in the lower panel of Figure 1 between 3 and 4 kHz at 17^h 23^m 49^s occur for specific wave vectors which depend only on the orientation and length of the antenna. These values of the wave vector at the nulls and their corresponding observed frequencies are used to determine the Doppler shifts of the ion waves. It will be shown that since the Doppler shift of a given wave vector can be measured, the dispersion relation in the rest frame of the plasma, $\omega_0(\vec{k})$, can be determined. The dispersion relation, wavelength, and direction of propagation are all used to single out ion acoustic waves propagating at an angle to the magnetic field as the only mode that can fit all observed characteristics.

II. ANTENNA INTERFERENCE EFFECTS

The first work on the explanation of the spectral features of short wavelength electrostatic waves was done by Gallagher [1982]. Gallagher's work was carried out on waves in the outer magnetosheath, where interference patterns very much like those found in Figure 1 were studied. Gallagher identified the interference patterns in the electric field data as an antenna effect caused by the presence of electrostatic waves with wavelengths shorter than the spacecraft electric field antenna.

To aid in understanding these interference effects it is useful to review the important features of the response of an electric dipole antenna to an electrostatic plane wave, following the development given by Gallagher [1982]. This development is similar to the theory developed by Temerin [1979] to explain antenna interference effects observed in low altitude satellites.

The potential between two points in space is given by

$$\Phi = -\int \vec{E} \cdot d\vec{s} \qquad .\tag{1}$$

The electic field of a plane, electrostatic wave, confined to the x − z plane, is given by

$$\vec{E} = (E_x\hat{x} + E_z\hat{z})e^{i\vec{k}\cdot\vec{r} - i\omega t} \quad .$$

If it is assumed for simplicity that the antenna is rotating in the x – y plane then

$$d\vec{s} = d\vec{\rho} \quad ,$$

$$\vec{E}\cdot d\vec{s} = E_x\cos \phi \, d\rho \quad ,$$

and

$$\vec{k}\cdot\vec{r} = k_x x = k_x\rho \cos \phi \quad ,$$

where ϕ is the azimuthal angle. The relevant geometry for this calculation is illustrated in Figure 2. Integrating Equation 1 from $-\ell/2$ to $\ell/2$ gives

$$\Phi = \frac{-2(E_x\cos \phi)\sin(k_x \frac{\ell}{2} \cos \phi)e^{-i\omega t}}{k_x\cos \phi} \quad . \tag{2}$$

The potential measured by the spacecraft depends on how the antenna responds to the electrostatic wave. If the antenna responds capacitively to the electrostatic wave and the capacitance per unit length

along the antenna is constant, then the potential measured by the
spacecraft is the average potential over one element of the antenna,

$$\overline{\phi} = \int_0^L \phi \, d\ell / \int_0^L d\ell \quad . \tag{3}$$

Upon integration and using the identity, $1 - \cos \alpha = 2 \sin^2 \alpha/2$, the
average potential of the antenna element is

$$\overline{\phi} = \frac{-8(E_x \cos \phi)}{L} \frac{\sin^2(\frac{k_x L \cos \phi}{4}) e^{-i\omega t}}{(k_x \cos \phi)^2} \quad . \tag{4}$$

The measured voltage, V_m, is proportional to the root mean square of
the average potential. Squaring Equation 4, averaging over one wave
period, and taking the square root gives

$$V_m \propto |E_x \cos \phi| \frac{\sin^2 x}{x^2} \quad , \tag{5}$$

where $\quad x = \dfrac{k_x L \cos \phi}{4} \quad .$

For waves with wavelengths $\lambda \gg L$ the $\sin^2 x/x^2$ term in Equation 5
approaches unity and the usual cosine spin modulation in the power
spectrum is obtained. If $\lambda \sim L$ then the $\sin^2 x/x^2$ term produces a

characteristic interference pattern that can be observed in the wide-
band data. To more thoroughly understand this term it is useful to
determine the minimum condition for the measured voltage. The minimum
in the measured voltage occurs when $\sin^2 x/x^2$ is zero. This condition
is met when

$$\frac{k_x L \cos \phi}{4} = m\frac{\pi}{2} \qquad m = 2, 4, \ldots \qquad (6)$$

Equation 6 is the final result desired and is used to determine Doppler
shifts of the ion waves. A simple explanation of the characteristic
shape of a typical interference pattern can be seen by rewriting Equa-
tion 6 as follows

$$Lk_x = \frac{2m\pi}{\cos \phi} \qquad (7)$$

For a fixed antenna position, from Equation 7, the condition for a
minimum, $(V_m = 0)$ is met when an integer number of wavelengths are pro-
jected onto the antenna. The average potential will be zero for an
integer number of projected wavelengths. Since the Doppler shift gives
a correspondence between the frequency and the wave vector, any pro-
jected wave vector which will give zero averaged power will correspond
to a null at a certain frequency in the wideband data. As the antenna
rotates and the angle ϕ between the projected wave vector and the
antenna approaches $\pm \pi/2$, larger and larger projected wave vectors are
required to meet the minimum condition. The pattern repeats every

one-half spacecraft rotation. The interference pattern is thus seen to provide the direction of the wave vector relative to the antenna.

The maximum measured voltage can also be used to determine the Doppler shift. The maximum measured voltage occurs when $\sin^2 x$ in Equation 5 equals one or when

$$\frac{k_x L \cos \phi}{4} = \frac{m\pi}{2} \qquad m = 1, 3, 5, \ldots \qquad (8)$$

It is important to realize that studying the interference patterns does not give any information about the component of the wave vector perpendicular to the spin plane. This information is lost when the dot product $\vec{E} \cdot \vec{ds}$ is taken to find the potential. This lack of information must be given careful consideration in wavelength estimations and measurements of the propagation direction. However, for the ISEE data the perpendicular component of the wave vector does not enter into the calculation of the Doppler shift because the spacecraft spin axis is oriented perpendicular to the plasma flow velocity so that $k_z V_{sw_z} = 0$.

III. CHARACTERISTICS OF THE UPSTREAM ION WAVES

Without making detailed calculations, much information about ion waves in the upstream region can be obtained from the identification and study of the interference patterns. The qualitative results in this section help further the understanding of the underlying physical processes that cause the interference patterns. In addition, some fundamental processes of waves in plasmas such as Doppler shift and Debye length are simply illustrated.

The first characteristic obtained from studying the wideband data is an estimation of the wavelengths of the upstream ion waves. To estimate the wavelengths one makes use of the fact that the ISEE-1 and -2 spacecraft are in nearly identical Earth orbits and on occasion are close enough together to observe nearly simultaneous upstream ion events. As pointed out in the introduction, the wideband receivers on ISEE-1 and -2 are essentially identical but the lengths of the electric dipole antennas on the spacecraft are different. As a result, differences in the wideband data for near simultaneous upstream ion events will be a result of the difference in the antenna response of the 215 meter dipole antenna on ISEE-1 as compared to the response of the 30 meter dipole antenna on ISEE-2.

As an example of the differences in the wave data, in Figure 3 the wideband frequency-time spectrograms are displayed for November 8, 1977

20^h 22^m U.T. The spacecraft location for the event was 17 R_E and 8.4^h magnetic local time. The separation of the two spacecraft was about 300 km. Protons travelling away from the bowshock at about solar wind speed take about one second to travel between the spacecraft, so the events occur nearly simultaneously at the two spacecraft. Comparing the two spectrograms in Figure 3 shows a general agreement in the change in frequency with time. The frequency-time wideband data for ISEE-1 clearly show evidence of interference patterns. For example, note the interference patterns centered around 20^h 22^m 15^s in the ISEE-1 wideband data. This observation of interference patterns in the ISEE-1 wideband data implies that the wavelength in the spin plane must be less than or approximately equal to 215 meters, the length of the ISEE-1 antenna.

Absence of interference patterns in ISEE-2 wideband data is an indication that the wavelength in the spin plane of the observed ion waves is not shorter than 30 meters, the length of the electric antenna on ISEE-2. This lower limit on the wavelength is in agreement with an approximate calculation of the Debye length for waves in the upstream region. The minimum wavelength allowed in a plasma is usually taken to be $\lambda_{min} = 2\pi \lambda_{De}$, which for the example in Figure 3 places λ_{min} at about 41 meters [Anderson et al., 1981]. This minimum wavelength is longer than the antenna length on ISEE-2, so interference patterns in the wideband data from this spacecraft should not be a common occurrence.

The lack of information on the component of the wave vector perpendicular to the spin plane means that one can only measure the

wavelength in the spin plane and not the actual wavelength of the ion
waves. However, the fact that interference patterns are frequently
observed in the wideband data from ISEE-1 implies that the actual wave-
length is not longer than the length of the ISEE-1 antenna. If the
actual wavelength was always much longer than the antenna one would
have to assume that the wave vector was always nearly perpendicular to
the spin plane of the spacecraft.

The qualitative evaluation presented above indicate a wavelength
between 30 and 215 meters for the ion waves. Anderson et al. [1981]
compared the electron field spectra for ISEE-1 and ISEE-2 and noted
that the ion wave spectral densities on ISEE-2, the spacecraft with the
shorter antenna, were greater than those on ISEE-1. From this observa-
tion, Anderson et al. concluded that ion waves in the upstream region
have wavelengths between 30 and 215 meters, in agreement with this
present study.

Another characteristic of the upstream ion waves is that the
direction of the wave vector does not change as a function of fre-
quency. One can show that the wave vector does not change as a func-
tion of frequency using the interference patterns observed in the wide-
band data. Consider in Figure 4 the interface between the two adjacent
interference patterns, indicated by an arrow at about 6^h 44^m 17.3^s.
The antenna of the spacecraft at this time is exactly perpendicular to
the spin plane projected wave vector. The null in the emission for all
frequencies at 6^h 44^m 17.3^s indicates that the antenna is perpendicular
to all spin plane projected wave vectors. This result indicates that
the azimuthal directions of the wave vectors are the same for all

frequencies. Although no information on the possible changes in k_z as a function of frequency can be obtained, it seems almost certain that the polar direction must also be independent of frequency. Otherwise, one would have to assume that the wave vector distribution is somehow determined by the z-axis orientation of the spacecraft.

In addition to wavelength determinations and wave vector direction considerations, the effects of the Doppler shift due to the motion of the solar wind can be illustrated. A good example of the effects of a Doppler shift on the interference patterns occurs on November 23, 1977 at 8^h 19^m U.T. and is illustrated in Figure 5. On November 23, the ISEE-1 spacecraft was located in the upstream region at a magnetic local time of about 9 hours and a radial distance of about 20 R_E. Starting from about 8^h 19^m 14^s U.T. the interference patterns retain their shape but shift downward in frequency as time progresses. This downshift can be understood by first considering the Doppler shift equation,

$$\omega'(\vec{k}) = \omega_0(\vec{k}) + \vec{k} \cdot \vec{V}_{sw} \qquad , \qquad (9)$$

which relates a given wave vector to a Doppler-shifted frequency. If the direction, or magnitude of the wave vector, or the solar wind velocity changes, then there is a change in the Doppler-shifted frequency. Most probably the frequency variations are caused by changes in the wave vector because the solar wind magnitude and direction are usually constant on time scales of seconds [W. C. Feldman, personal

communication, 1983]. Detailed analysis of the wave vector direction, which will be described in the next section, indicates that the direction of the wave vector with respect to the solar wind velocity shifted from 8^h 19^m 14^s to 8^h 19^m 18.4^s. This shift in direction caused a change in the Doppler shift for all wavelengths present. The fact that the Doppler-shifted frequency can change over a period of a few seconds is an indication that the wave vector of the electrostatic waves is highly variable.

A final example of characteristics of the ion waves deals with how the spectrum of the electric field emissions changes when ISEE-1 enters the outer magnetosheath. A good example of the change in the interference patterns is presented in Figure 6. In this figure the orbit of ISEE-1 projected into the equatorial plane is combined with examples of the wideband data from the upstream region at 6^h 56^m and from the outer magnetosheath at 9^h 25^m. The ion waves observed in the outer magnetosheath on this day were studied in detail by Gallagher [1982] and have the same characteristics as the ion waves observed in the upstream region. A major difference in the appearance of the wideband data is that the magnetosheath ion waves are only Doppler shifted to 4 kHz. The ion waves in the upstream region on the same pass show Doppler shifts up to 10 kHz. This difference in Doppler shift can be easily understood because the two regions of interest have different plasma flow velocities and directions. The solar wind velocity on November 22, 1977, is on the order of 300 km/sec [W. C. Feldman, personal communication, 1983], and is directed almost antisunward. An

estimate of the minimum wavelength allowable using the electron temper-
ature in Appendix B for the upstream region is about 50 meters.   This
minimum wavelength results in a maximum Doppler shift from zero rest
frame frequency of about 7 kHz.   This upper cutoff frequency should be
compared with the wideband data in Figure 6 at 8^h 56^m.   The upper cut-
off frequency is not in exact agreement with Figure 6 as the electric
field emissions are observed at frequencies as high as 10 kHz.   One
reason there is not exact agreement is that the rest frame frequency
will be shown in the next section to be greater than zero.   In the mag-
netosheath for the same day at 9^h 25^m the bulk flow velocity was around
160 km/sec and the minimum wavelength from typical plasma parameters
for that region was around 36 meters [Gallagher, 1982].   Furthermore,
in the magnetosheath there was a large shift in the direction of the
bulk plasma flow velocity away from the antisunward direction.   These
approximate parameters result in a maximum Doppler shift on the order
of 4 kHz.   This upper cutoff frequency should be compared with the fact
that no emissions are observed above 4 kHz in Figure 6 at 9^h 25^m.   The
above comparison shows good relative agreement with the Doppler shift
character of the ion waves.   In the next section more detailed analysis
of the direction of propagation and Doppler shift of the waves in the
upstream region will be considered.

IV.   DIRECTION OF PROPAGATION AND DOPPLER SHIFT

The direction of propagation of the upstream ion waves was first studied by Anderson et al. [1981]. Anderson's measurements made use of spacecraft spin modulation, not interference patterns. The measurements were difficult to make because the intensity often fluctuates rapidly when compared to the spin period. The ion waves are also observed to shift in direction sometimes on the order of a few tenths of a second, much less than the few seconds required to determine spin modulation. When the measurements of the direction of propagation could be made it was concluded, except for a few anomalous cases, that the peak amplitudes in the electric field were most nearly aligned parallel to the ambient magnetic field [Anderson et al., 1981].

By using spin-modulated interference patterns in the wave data, the wave vector direction projected into the spin plane can be determined very accurately. The projected wave vector direction is then compared to the magnetic field direction projected into the spin plane.

In order to determine the wave vector direction the angle between the antenna and some reference point is required. The reference point used in this study is the sun. The sun-antenna angle is an engineering parameter which can be obtained from the data tape. First, one must determine the time of minimum (or maximum) frequency of an interference pattern. The minimum frequency of the interference pattern occurs when

the antenna is oriented parallel to the wave vector projected into the spin plane (or perpendicular to the wave vector direction in the case of the maximum in frequency) as demonstrated in Figure 7. The sun-antenna angle for the minimum in frequency is the sun-wave vector angle. The magnetic field-sun angle is determined by interpolation of high resolution magnetic field data obtained from the magnetometer on ISEE-1 and provided by C. Russell. The sun-wave vector angle is then compared to the sun-magnetic field angle. If the wave vector is parallel to the magnetic field, then the difference of the sun-wave vector angle and the sun-magnetic field angle should always be near zero. Projection effects due to the lack of knowledge of the perpendicular component of the wave vector cause ambiguous results if the wave vector is not parallel to the magnetic field. In order to reduce the problem of projection effects, events were selected when the spacecraft z component of the magnetic field was very nearly zero.

The wave vector direction was determined using interference patterns observed at two different time periods, November 8, 1977, 20^h 12^m to 20^h 27^m and November 23, 1977, 8^h 14^m to 8^h 20^m. A total of 88 separate interference patterns were studied. The results of the study of these time periods indicate that the wave vector direction is not simply aligned parallel to the magnetic field. The distribution of angles between the projected magnetic field for November 23, 1977, 8^h 14^m to 8^h 20^m is given in Figure 8a. The angle between the spin plane projected wave vector and the spin plane projected magnetic field is not observed to be near zero. Out of the 88 interference patterns studied, eight cases coincided with times when the magnitude of the

spacecraft z component of the magnetic field was less than 1% of the total magnitude of the magnetic field. The distribution of angles for the eight events is presented in Figure 8b. The lack of large angles between the spin plane projected wave vector and the magnetic field in Figure 8b indicates that the wave vector is also not perpendicular to the magnetic field. A more detailed example of the geometry for a particular event on November 8, 1977, at 20^h 27^m 33.4^s is illustrated in Figure 9. On November 8, 1977, 20^h 27^m 33.4^s the angle between the wave vector and the magnetic field was 39 degrees. At this time, the spacecraft z component of the magnetic field from the magnetometer data was less than 3% of the total magnitude of the magnetic field. If the wave vector was perpendicular to the magnetic field, then the z component of the wave vector would have to be extremely large to account for the projection of the wave vector onto the spin plane to be at such a small angle to the magnetic field.

Typical values of the angle between the spin plane projected magnetic field and the spin plane projected wave vector range from 10 degrees to 75 degrees and usually average $40° \pm 20°$. This result is in contrast to the near parallel propagation reported by Anderson et al. [1981].

In addition to measurements of the direction of propagation, the Doppler shift of the ion waves in the upstream region can be readily measured using the interference patterns observed in the wave data. A measurement of the rest frame frequency of the waves can be obtained by subtracting the Doppler shift from the frequency measured by the spacecraft.

To determine the Doppler shift of a wave the relation between the observed frequency of the waves and the wavelength of the wave is required. To understand the frequency-wavelength correspondence, consider the equation for the Doppler shift (Equation 9) in detail.

$$\omega'(\vec{k}) = \omega_0(\vec{k}) + \vec{k} \cdot \vec{V}_{sw} \qquad , \qquad (9)$$

In Equation 9 there are three terms. Each term has certain very important properties. The first term, $\omega'(\vec{k})$ is simply the frequency observed on the wideband frequency-time spectrogram. The observed frequency depends on the wave vector through the rest frame frequency and the Doppler shift. The second term, $\omega_0(\vec{k})$ is the rest frame frequency. The rest frame frequency depends on the wave vector through the dispersion relation for the waves. The dispersion relation depends on the plasma wave mode. Since the mode of propagation of the ion waves has not been conclusively identified, the wave vector dependence of $\omega_0(\vec{k})$ is not known. The third term in Equation 9 is the Doppler shift term. It depends on the magnitude of the wave vector and its direction of propagation relative to the solar wind. This third term can be calculated using information obtained from the study of interference patterns observed in the wideband data. To determine the Doppler shift, note first that when interference patterns are analyzed, only wave magnitudes and directions projected into the spin plane are obtained. No information about the contribution of the $k_z V_{sw_z}$ term to the Doppler shift in Equation 9 can be obtained. Fortunately, the

solar wind velocity is always very close to the antisunward direction.
Since the spin axis of ISEE-1 is perpendicular to the ecliptic plane,
the solar wind is rarely more than one degree out of the spacecraft
spin plane, therefore $V_{sw_z} \approx 0$. This simplifies the Doppler shift
equation to

$$\omega(\vec{k}) = \omega_0(\vec{k}) + \vec{k}_\rho \cdot \vec{V}_{sw\rho} \tag{10}$$

where k_ρ is the spin plane projected wave vector. Because $|\vec{k}_\rho|$ and the
angle between $\vec{k}_\rho$ and $\vec{V}_{sw_\rho}$ can be measured at the nulls in the inter-
ference pattern, the Doppler shift for these wave vectors can be com-
puted exactly.

In order to determine the Doppler shift, the frequency and time of
occurrence of a null in the wideband spectrum of a particular inter-
ference pattern is determined, as in Figures 4 and 6. The projected
wave vector for the null in intensity is given by Equation 7 to be

$$k_\rho = \frac{2m\pi}{L \cos \phi} \cdot \tag{11}$$

This projected wave vector depends only on the antenna length and the
direction of the projected wave vector relative to the antenna. When
the antenna is aligned along the projected wave vector as in Figure 7,
then ϕ is zero so that

$$k_{\rho Null} = \frac{2m\pi}{L} \qquad\qquad m = 2, 4, \ldots \qquad\qquad (12)$$

The equation for the frequency of these projected wave vectors is then

$$\omega'(\vec{k}) = \omega_0(\vec{k}) + \frac{2m\pi}{L} |\vec{V}_{sw}| \cos \psi \qquad . \qquad\qquad (13)$$

Similarly, the Doppler shift equation for a maximum in intensity, obtained from Equations 8 and 10, is

$$\omega'(\vec{k}) = \omega_0(\vec{k}) + \frac{2m\pi}{L} |\vec{V}_{sw}| \cos \psi \qquad m = 1, 3, 5, \ldots \qquad (14)$$

The angle ψ between the projected wave vector and the solar wind can be obtained by measuring the time of the minimum in frequency of the interference pattern exactly the same way as the direction was obtained for the measurements of the direction of propagation.

Since all quantities in either Equations 12 or 13, except for the rest frame frequency, are known for a particular value of m, the rest frame frequency can be calculated. If enough nulls or maximums at different frequencies are observed, one can experimentally determine the dispersion relation for certain specific wave vectors. The dispersion relation cannot be determined completely because the component of the wave vector perpendicular to the spin plane is not known.

The event selected to illustrate the determination of the dispersion relation occurred on November 22, 1977, at $6^h 44^m 15^s$. At this

time ISEE-1 was located in the upstream region at about 16.8 R_E and
10.3 hours magnetic local time. Figure 6 is an equatorial projection
of the ISEE-1 orbit for this day. The particular event at 6^h 44^m was
chosen because the antenna interference patterns in the wideband data
very clearly show the nulls in intensity at three different frequencies
and the maximums in intensity at three frequencies. The identification
of the three nulls in intensity is shown in Figure 4.

The nulls and maximums in intensity and the time of occurrence of
the nulls and maximums were not measured from the wideband film. The
limited dynamic range of the wideband film (at best 20 db) and the
difficulty in determining precise times and frequencies would cause
uncertainties which would be too large to make measurements of the rest
frame frequency meaningful. Instead, electric field intensity versus
frequency plots of the original digitized wideband data were made at 50
millisecond intervals by computer to reproduce the event with much more
accuracy in time and frequency. An example of 7 of the intensity ver-
sus frequency computer plots centered around 6^h 44^m 17.9^s is pre-
sented in Figure 10. The nulls corresponding to $k_\rho Null = \frac{4\pi}{L}$ and
$k_\rho Null = \frac{8\pi}{L}$ are identified. The particular geometry for the event
obtained from the study of the computer generated plots of the event is
illustrated in Figure 11. The solar wind velocity on November 22,
1977, at 6^h 44^m was 307 km/sec [W. C. Feldman, personal communication,
1983]. The results from the study of the event are presented in Table
1. The rest frame frequencies are listed as positive by convention.
The uncertainty in the rest frame frequencies are a result of a $\pm 6°$
uncertainty in the direction of the spin plane projected wave vector,

Table 1

Observed and Calculated Frequencies for
November 22, 1977, 6^h 44^m 18^s

m	Wave No. (m^{-1})	Observed Frequency kHz	Doppler Shift kHz	Rest Frame Frequency Hz
1	.0292	1.1 ± .1	−1.43	330 ± 100
2	.0584	2.3 ± .1	−2.85	550 ± 110
3	.0877	3.6 ± .1	−4.28	680 ± 120
4	.1169	4.9 ± .1	−5.70	800 ± 140
5	.1461	6.2 ± .1	−7.13	930 ± 160
6	.1753	7.7 ± .1	−8.46	760 ± 220

an uncertainty of ±.1 kHz in the observed frequency, and an uncertainty
of ±5 km/sec in the solar wind velocity. The uncertainty in determin-
ing the frequency of the nulls and the maximums and their time of oc-
currence must be minimized because small uncertainties in the observed
frequency or the Doppler-shifted frequency cause large uncertainties in
the rest frame frequency. A more detailed presentation of the calcula-
tion of the uncertainties is given in Appendix A. The ion plasma fre-
quency at 6^h 44^m was computed from the observed electron plasma fre-
quency to be about 800 Hz. The rest frame frequencies listed in Table
1 are on the order of the ion plasma frequency. This result, along
with the wave vector direction and magnitude observations, is summa-
rized in the next section and used to identify the plasma wave mode.

V. INTERPRETATION

Three results from the study of interference patterns in the wide-
band data place important constraints on any theory that attempts to
explain the production of the ion waves in the upstream region. The
results can be summarized as follows:

1. The wavelength of the ion waves is on the order of $2\pi\ \lambda_{De}$.

2. The wave vector of the ion waves is neither parallel nor per-
pendicular to the magnetic field. The ion waves are observed to be
propagating at an average angle of $40° \pm 20°$ from the magnetic field.
The wave vector direction is the same for all frequencies.

3. The ion waves are Doppler shifted by the solar wind into a
frequency range of $1 - 10$ kHz. The rest frame frequency increases with
increasing wave vector magnitude. The maximum rest frame frequency is
on the order of the ion plasma frequency.

The above three results can be used to rule out a number of plasma
wave modes. Buneman waves [Rodriguez, 1981] can be ruled out because
the wavelengths required are many times the Debye length and would not
produce antenna interference patterns in the ISEE-1 data. Bernstein
waves can be shown to be heavily damped for angles other than nearly
perpendicular propagation. Waves excited by the density gradients [Wu
et al., 1982] have the correct frequency, but these waves propagate
perpendicular to the magnetic field and have wavelengths many times the

Debye length, which is not consistent with the observational results of this study. Whistler mode waves are observed in the upstream region at frequencies up to about 200 Hz, which is on the order of the ion plasma frequency, [Smith et al., 1967; Anderson et al., 1981]. However, whistler mode waves have wavelengths many times the Debye length and would not produce interference patterns in the wideband data.

The wave mode that fits all observations is the ion acoustic mode. Ion acoustic waves are characterized by short wavelengths, $\lambda \gtrsim 2\pi \lambda_{De}$, which agrees with the short wavelengths observed. Ion acoustic waves have frequencies $\omega < \omega_{pi}$, which agrees with the rest frame frequencies listed in Table 1. For very long wavelengths, the phase velocity of the ion acoustic waves is $C_s = \omega/k$, where $C_s = \sqrt{\dfrac{kT_e}{m_i}}$ is called the ion acoustic speed. For the event on November 22, 1977, the electron temperature was $1.6 \times 10^5 K$ [W. C. Feldman, personal communication, 1983]. The ion acoustic speed for this event is then $C_s = 36$ km/sec. Considering the first entry in Table 1, $f_0 = 330$ Hz and $k_\rho = .0292$ m^{-1}, the measured phase velocity is $\dfrac{\omega_0}{k_\rho} = 70$ km/sec, which is about a factor of 2 larger than the ion acoustic speed. The measured phase velocity is expected to be greater than the ion acoustic speed because to obtain the phase velocity the rest frame frequency is divided by k_ρ and not $k = \sqrt{k_\rho^2 + k_z^2}$. Ion acoustic waves can propagate at angles to the magnetic field [Tidman and Krall, 1971], so the measurements of the direction of propagation in this study are not inconsistent with the identification of the upstream ion waves as ion acoustic waves. The next step is to compare the dispersion relation for ion acoustic waves with the computed rest frame frequencies and wave vectors listed in Table 1.

Krall and Trivelpiece [1973] derived a relationship between frequency and wave number for ion acoustic waves. The derivation uses linear Vlasov theory with Maxwellian velocity distributions and assumes weak damping. The dispersion relation is

$$\omega^2 = \frac{k^2 C_s^2}{1 + k^2 \lambda_{De}^2} \tag{15}$$

where $C_s = \sqrt{\frac{kT_e}{m_i}}$, is the ion acoustic speed. For long wavelengths, $k\lambda_{De} \ll 1$, Equation 15 becomes

$$\omega^2 = k^2 C_s^2 \quad . \tag{16}$$

That is, all waves travel at the ion acoustic speed. For very short wavelengths, $k\lambda_{De} \gg 1$, Equation 15 becomes

$$\omega^2 = \frac{C_s^2}{\lambda_{De}^2} = \omega_{pi}^2 \quad . \tag{17}$$

The fact that $\omega < \omega_{pi}$ suggests normalization of Equation 15 by the ion plasma frequency to get the normalized dispersion relation

$$\frac{\omega^2}{\omega_{pi}^2} = \frac{k^2\lambda_{De}^2}{1 + k^2\lambda_{De}^2} \quad . \tag{18}$$

To compare this dispersion relation to the quantities listed in Table 1, the value of k_z must be known. This quantity cannot be found using interference patterns. However, it was shown that the wave vector direction is independent of frequency. From this result, one can write

$$k_z = k_\rho \tan\theta \quad , \tag{19}$$

where θ is the angle that the wave vector makes with respect to the spacecraft spin plane. Equation 18 can now be rewritten as

$$\frac{\omega^2}{\omega_{pi}^2} = \frac{k_\rho^2\lambda_{De}^2\sqrt{1 + \tan^2\theta}}{1 + k_\rho^2\lambda_{De}^2\sqrt{1 + \tan^2\theta}} \quad . \tag{20}$$

A plot of ω/ω_{pi} versus $k_\rho\lambda_{De}$ for various values of θ is presented in Figure 12.

Also in Figure 12 are the wave number-rest frame frequency points listed in Table 1. In order to normalize the observed values of rest frame frequency and projected magnitude of the wave vector, the Debye length and the ion plasma frequency on November 22, 1977, had to be known. These normalized parameters are calculated from measured plasma

parameters in Appendix B. From Figure 12 one can see that the observed frequencies and projected wave vectors fit the ion acoustic dispersion relation if one assumes that the wave vector is 60° out of the spin plane. The close agreement of the observed data with the characteristic shape of the ion acoustic dispersion relation is a strong indication that the ion waves observed upstream of the Earth's bowshock are ion acoustic waves.

VII. DISCUSSION AND CONCLUSIONS

The final result of this study is that the waves observed in the region upstream of Earth's bowshock in the frequency range of 1 to 10 kHz are Doppler-shifted ion acoustic waves. This result is the same conclusion reached by Gurnett and Frank [1978] and Anderson et al., [1981]. The work by Anderson et al. used the same data but different methods to arrive at wavelength and measurements of the direction of propagation. This study used more powerful methods to determine wave vector direction and wavelength and went beyond the studies by Gurnett and Frank and by Anderson et al. by determining the frequency range and general shape of the dispersion curve. Along with the results of the studies by Gurnett and Frank and by Anderson et al., this study now adds overwhelming evidence in favor of ion acoustic waves.

With the results of this study the production of ion acoustic waves by an ion beam instability must be reconsidered. Using Figures 2 and 3 from Lemons et al. [1979], Gary [1981] notes that an ion beam drives the ion acoustic instability with the wave vector parallel to the magnetic field only if $3 < v_b/v_i < 10$ and $T_e/T_i > 5$, where v_b is the velocity of the beam and v_i is the ion thermal velocity. However, the wave vector has now been shown to be at a substantial angle to the magnetic field. To account for propagation at angles to the magnetic field, it can be shown using linear Vlasov theory that v_b is replaced

by $v_b \cos \theta$ [Tidman and Krall, 1971], where θ is the angle between the wave vector and the magnetic field. The wave vector direction can now be adjusted so that the condition $3 < v_b \frac{\cos \theta}{v_i} < 10$ is met. For typical values, $v_b = 400$ km/sec and $v_i = 20$ km/sec, given by Gary [1981] the minimum angle is $\theta_{min} = 60°$ which is not inconsistent with the directions of propagation found in this study. This calculation does not demonstrate instability because the other condition, $T_e/T_i > 5$, is not observed in the upstream region. However, the fact that the wave vector is not parallel to the magnetic field improves the possibility of generation of the ion waves in the upstream region by the ion beam instability.

The new measurements of the direction of propagation of the ion waves do not rule out the possibility of generation of ion waves by the heat flux instability [Forslund, 1970]. Tidman and Krall [1971] show that instability occurs for wave numbers such that $\frac{\omega}{k} < v_b \cos \theta$. This condition produces a cone of unstable phase velocity vectors centered around the magnetic field. However, the heat flux instability requires a T_e/T_i ratio greater than 10, which is not observed in the upstream region.

The identification of ion waves as ion acoustic waves brings to an end the study of these upstream waves using wave data alone. Clearly, the next step to understanding the mechanism of the instability is more detailed study combining wave and particle data similar to the studies done by Scarf et al. [1970] and Anderson et al. [1981]. One exciting prospect involves the gyrophase bunched ions observed upstream of the bowshock [Eastman et al., 1981; Gurgiolo et al., 1981]. It would

be very interesting to know if the wave vector direction of the ion acoustic waves has any correlation with the direction of the gyrophase bunched ions. This possibility can be explored using existing wave and particle data. Another possibility of joint wave and particle studies is to determine how the observed frequency of the ion acoustic waves changes with changes in the velocity of the backstreaming ions. These are just two of the possibilities of wave and particle correlations that would shed more light on the problem of production of the ion acoustic waves in the upstream region.

Other regions of space where the techniques presented in this study are applicable are in the bowshock and in the solar wind. Inside the bowshock, particle distributions unstable to ion acoustic waves are known to exist [Feldman et al., 1982]. The wave vector direction of these ion acoustic waves could possibly be measured. Also, ISEE-1 is occasionally in regions where it is in the solar wind but not on a field line connected to the bowshock. In the solar wind, ion acoustic waves are also believed to exist [Gurnett and Anderson, 1977; Gurnett and Frank, 1978]. If these solar wind ion acoustic waves can be observed using wideband measurements, the methods presented in this study can be used to determine wave vector direction and Doppler shift.

In summary, the results of this study answer some important questions and open up possibilities of new aproaches to the important question of generation of ion acoustic waves. The methods used in this study are limited to wavelengths shorter than the spacecraft antenna length. Fortunately, there are enough important questions to be answered where these methods are applicable.

REFERENCES

Anderson, R. R., C. C. Harvey, M. M. Hoppe, B. T. Tsurutani, T. E. Eastman, and J. Etcheto, Plasma waves near the magnetopause, J. Geophys. Res., 87, 2087-2107, 1982.

Anderson, R. R., G. K. Parks, T. E. Eastman, D. A. Gurnett, and L. A. Frank, Plasma waves associated with energetic particles streaming into the solar wind from the Earth's bowshock, J. Geophys. Res., 86, 4493-4510, 1981.

Bevington, P. R., Data Reduction and Error Analysis for the Physical Sciences, McGraw-Hill, 1969.

Eastman, T. E., R. R. Anderson, L. A. Frank, and G. K. Parks, Upstream particles observed in the earth's foreshock region, J. Geophys. Res., 86, 4379, 1981.

Feldman, W. C., R. C. Anderson, S. J. Bame, S. P. Gary, J. T. Gosling, D. J. McComas, M. F. Thomsen, G. Paschmann, and M. M. Hoppe, Electron velocity distributions near the Earth's bowshock, J. Geophys. Res., 88, 96, 1983.

Forslund, D. W., Instabilities associated with heat conduction in the solar wind and their consequences, J. Geophys. Res., 75, 17, 1970.

Gallagher, D. L., Short wavelength electrostatic waves in the Earth's magnetosheath, Ph.D. Dissertation, University of Iowa, 1982.

Gallagher, D. L., Short wavelength electrostatic waves in the Earth's magnetosheath, J. Geophys. Res., submitted, 1982.

Gary, S. P., Ion-acoustic-like instabilities in the solar wind, J. Geophys. Res., 83, 2504, 1978a.

Gary, S. P., Microinstabilities upstream of the Earth's bowshock: A brief reivew, J. Geophys. Res., 86, 4331, 1981.

Gurgiolo, C., G. K. Parks, B. H. Mauk, C. S. Lin, K. A. Anderson, R. P. Lin, and H. Reme, Non-ExB ordered ion beams upstream of the Earth's bowshock, J. Geophys. Res., 86, 4415, 1981.

Gurnett, D. A., and R. R. Anderson, Plasma wave electric fields in the solar wind: Initial results from Helios 1, J. Geophys. Res., 82, 632, 1977.

Gurnett, D. A., and L. A. Frank, Ion acoustic waves in the solar wind, J. Geophys. Res., 83, 58, 1978.

Gurnett, D. A., F. L. Scarf, R. W. Fredricks, E. J. Smith, The ISEE-1 and ISEE-2 plasma wave investigation, IEEE Trans. Geosci. Electr., GE-16, 225, 1978.

Krall, Nicholas A., and Alvin W. Trivelpiece, Principles of Plasma Physics, McGraw-Hill, 1973.

Lemons, D. S., J. R. Asbridge, S. J. Bame, W. C. Feldman, S. P. Gary, and J. T. Gosling, The source of electrostatic fluctuations in the solar wind, J. Geophys. Res., 84, 2135, 1979.

Rodriguez, P., Ion waves associated with solar and beam-plasma interactions, J. Geophys. Res., 86, 1279-1289, 1981.

Scarf, F. L., R. W. Fredricks, L. A. Frank, C. T. Russell, P. J. Coleman, Jr., and M. Neugebauer, Direct correlations of large amplitude waves with suprathermal protons in the upstream solar wind, J. Geophys. Res., 75, 7316, 1970.

Smith, E. J., R. H. Holzer, M. G. McLeod, and C. T. Russell, Magnetic noise in the magnetosheath in a frequency range 3-300 Hz, J. Geophys. Res., 72, 4803, 1967.

Temerin, Michael, Doppler shift effects on double-probe measured electric field power spectra, J. Geophys. Res., 84, 5929-5934, 1979.

Tidman, D. A. and Nicholas A. Krall, Shock Waves in Collisionless Plasmas, Wiley, 1971.

APPENDIX A

ANALYSIS OF UNCERTAINTIES

ANALYSIS OF UNCERTAINTIES

The uncertainties listed in Table 1 for the rest frame frequency were obtained in the following way.

Assuming the uncertainties in measuring the wave direction and magnitude and in measuring the magnitude of the solar wind are uncorrelated one can use propagation of errors [P. R. Berington, 1969] to arrive at the following equation for the error in determining the rest frame frequency of oscillation from the Doppler shift formula (Equation 12).

$$(df_o(k_{\rho Null}))^2 = (df'(k_{\rho Null}))^2 + (\frac{|V_{sw}|}{2\pi} \cos \psi \, dk_{\rho Null})^2$$

$$+ (\frac{k_{\rho Null}}{2\pi} \cos \psi \, d|V_{sw}|)^2 + (\frac{k_{\rho Null}|V_{sw}|}{2\pi} \sin \psi \, d\psi)^2 \quad .$$

(A1)

The quantity $dk_{\rho Null}$ is equal to zero because, from the theory of dipole antenna response, the value of $k_{\rho Null} = \frac{2m\pi}{L}$ is known exactly. (That is, assuming the length of the antenna is known with a high degree of accuracy.) The solar wind direction was assumed to be exact. Equation A1 reduces to

$$(df_o(k_{\rho Null}))^2 = (df'(k_{\rho Null}))^2 + (\frac{k_{\rho Null}}{2\pi} \cos \psi \, d|V_{sw}|)^2$$

$$+ (\frac{k_{\rho Null}|V_{sw}|}{2\pi} \sin \psi \, d\psi)^2 \quad . \tag{A2}$$

In order to reduce the errors in the determination the time of minimum frequency (which leads to the uncertainties in the angle ψ), and also to reduce the uncertainties in determining the observed frequency of the wave for a particular $k_{\rho Null}$, the wave data was plotted with the aid of a computer using very high time and frequency resolution. The location of $k_{\rho Null}$ and the time was then determined with sufficient accuracy by eye from the computer generated plots of the wave data. The error in the solar wind velocity was estimated to be ± 5 km/sec. The solar wind velocity is usually determined within a couple of percent, so this estimate is about right.

As an example, consider the second value for the uncertainty in the rest frame frequency listed in Table 1. The estimate of the uncertainty in the angle ψ (from the estimate in the uncertainty in the time of minimum in frequency) and the uncertainty in the observed frequency of oscillation for this time were found to be

$$d\psi = \pm 6°$$

and

$$df' = \pm .1 \text{ kHz}$$

Putting these values into Equation A2, with $\psi = 5°$, $k_{\rho Null} = \frac{2m\pi}{L}$, and $|V_{sw}| = 307$ km/sec one finds

$$(df_o(k_{\rho Null} = \frac{4\pi}{L}))^2 = .01 + .0190 + .0197 \text{ (kHz)}^2 \qquad \text{(A3)}$$

and finally

$$df_o(k_{\rho Null} = \frac{4\pi}{L}) = \pm .220 \text{ kHz} \qquad \text{(A4)}$$

APPENDIX B

MEASURED AND COMPUTED PLASMA PARAMETERS

FOR NOVEMBER 22, 1977

MEASURED PARAMETERS

density $\qquad n = n_e \approx 15 \text{ cm}^{-3}$

(This number is a compromise between particle measurements, which obtains too high an estimate, and an estimate of the density from the wave data.)

electron temperature $\qquad T_e \approx 1.6 \times 10^5 \text{K}$

[W. C. Feldman, personal communication, 1983]

COMPUTED PARAMETERS

Ion plasma frequency $\qquad$ $\omega_{pi} = 5{,}130/\text{sec}$

Electron Debye length $\qquad$ $\lambda_{De} \simeq 7 \text{ meters}$

Ion acoustic speed $\qquad$ $C_s = 36 \text{ km/sec}$

APPENDIX C

FIGURES

Figure 1   Wideband data from the ISEE-1 spacecraft on December

24, 1977, (day 358) illustrate the characteristic

short wavelength, antenna interference effects on ion

waves in the upstream region. The spacecraft was

located at about 22 R_E, and 6.1 hours magnetic local

time. The upper panel shows the characteristic shape

of the electric field emissions and their relation to

the spin of the spacecraft. The lower panel is the

wideband data where higher electric field intensities

are shown as darker shading. The periodic rise and

fall in frequency is directly related to the space-

craft spin. The null in intensity between 3 and 4 kHz

centered around $17^h\ 23^m\ 49^s$ occurs for a specific wave

vector.

B-G83-175
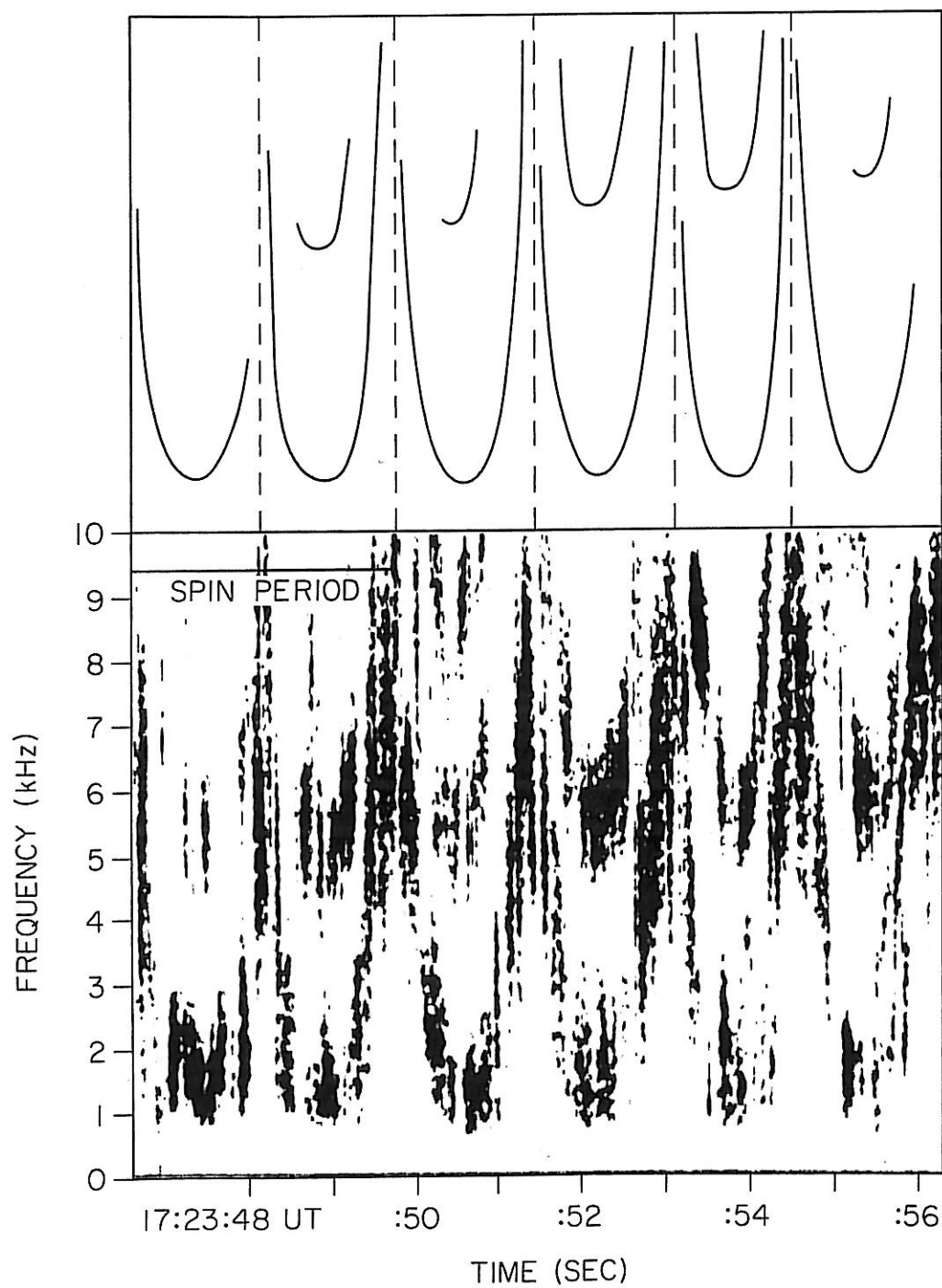
ISEE-I WIDEBAND DATA

Figure 1

Figure 2   The geometry used to understand the antenna response
to an electrostatic wave. The electric field, E
and the wave vector, k are in the x-z plane. The
spacecraft antenna spin axis is in the $\hat{Z}$ direction.
The terms E_x and k_x are the spin plane projected
electric field and wave vector. $E_x \cos \phi$ and $k_x \cos \phi$
are the spin plane projected electric field and wave
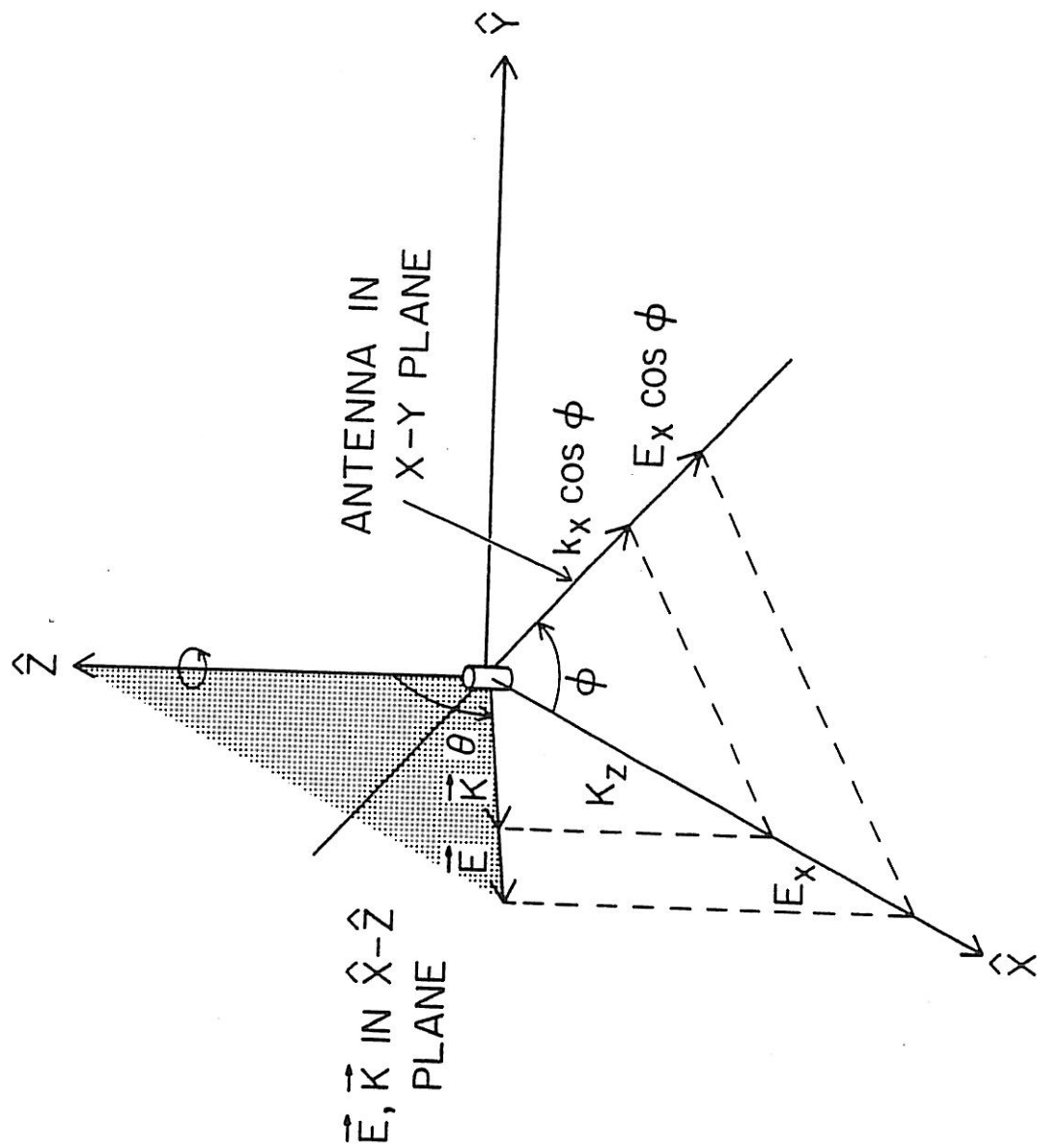vector projected onto the antenna.

A-G83-218

Figure 2

Figure 3 A comparison of wideband data from the ISEE-1 and -2

spacecraft is displayed. The spacecraft were located

in the upstream region about 300 km apart. The

upstreaming protons from the bow shock, which are

thought to trigger the ion wave instability travel

the 300 km in about one second. The gereral struc-

ture of the increase and decrease in frequency

observed in the wideband data is the same for the two

spacecraft with the exception that ISEE-2 appears to

have an overall shift of about one second. However,

detailed structure such as the antenna interference

patterns centered around $20^h\ 22^m\ 15^s$ for ISEE-1 are

absent in the ISEE-2 wideband spectrograms.

A-G83-115

WIDEBAND DATA

NOVEMBER 8, 1977   DAY 312   ORBIT 8

R=17.1 R$_E$ MAG LAT=22.1°   MLT=8.4 HRS

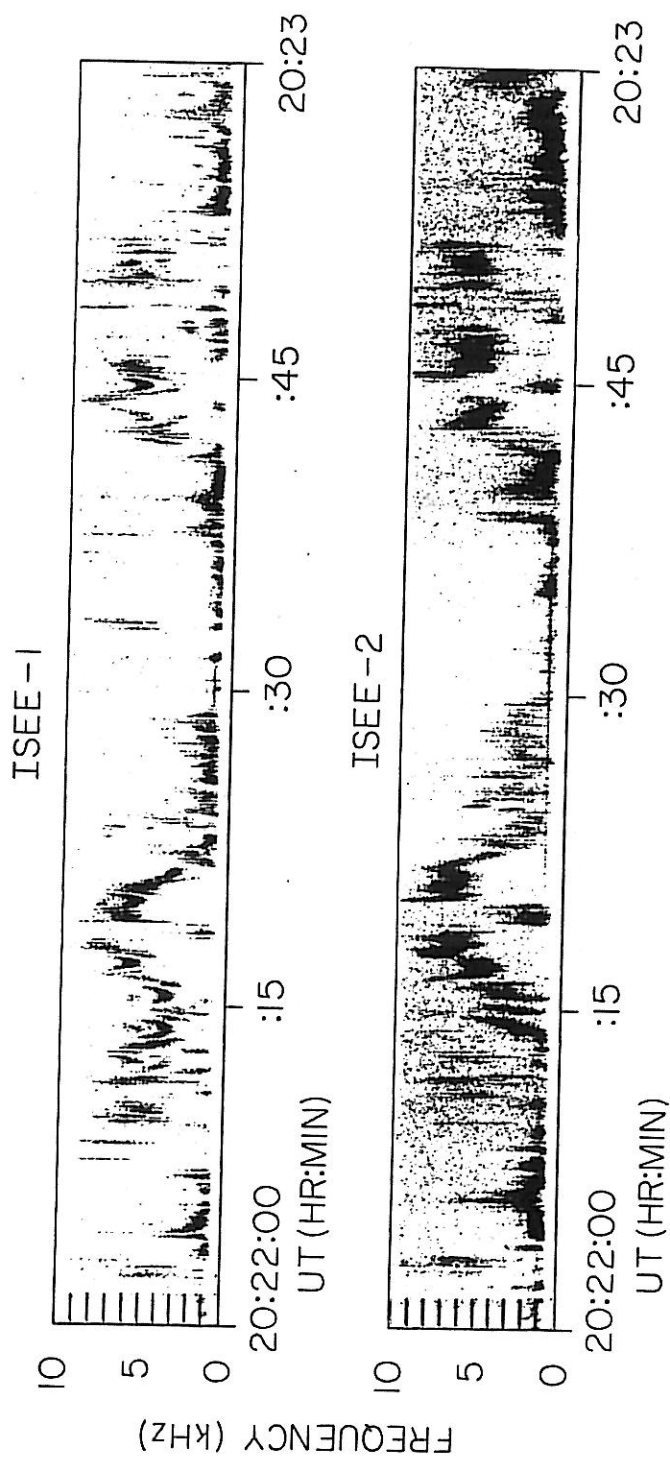SPACECRAFT SEPARATION = 296 KM

Figure 3

Figure 4   Wideband data on November 22, 1977, used to show that

the wave vector direction is the same for all fre-

quencies. On November 22, 1977, (day 326) ISEE-1 was

located in the upstream region at 10.3 hours magnetic

local time and at a distance of about 16.8 R_E.

Notice the sharp division between the interference

patterns identified by the arrow at about 6^h 44^m

17.3^s. This sharp division at all frequencies indi-

cates that the direction of the wave vector is the

same for all frequencies. This event is used for the

calculation of the Doppler shift of the ion waves.

The nulls identified and their time of occurrence

give the frequency-wave vector relationship required
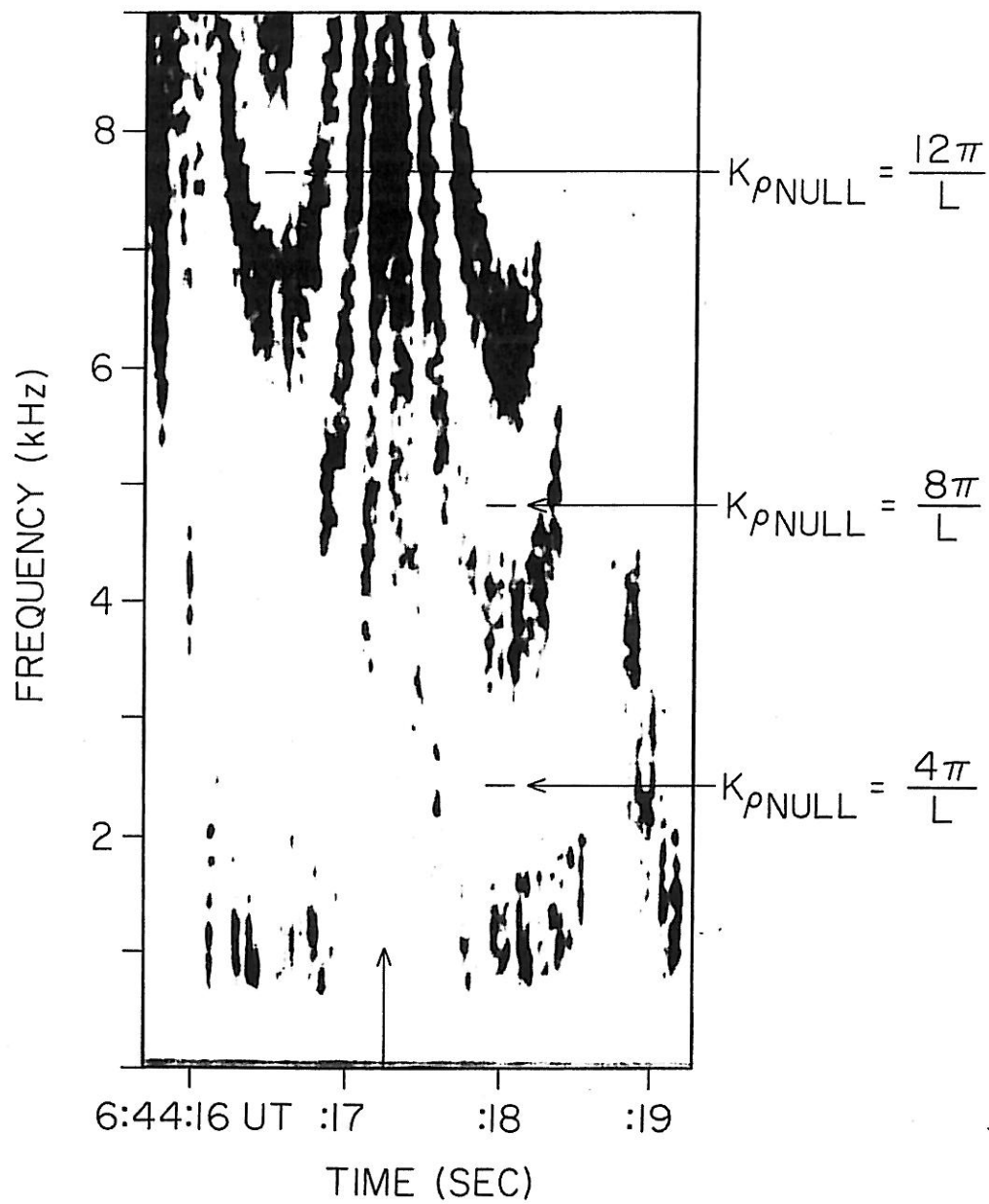
for the equation for the Doppler shift.

A-G83-146-1

ISEE-1 WIDEBAND DATA
YEAR 1977 DAY 326

$K_{\rho NULL} = \dfrac{12\pi}{L}$

$K_{\rho NULL} = \dfrac{8\pi}{L}$

$K_{\rho NULL} = \dfrac{4\pi}{L}$

Figure 4

Figure 5   ISEE-1 wideband frequency-time spectrogram showing

the effect of the Doppler shift on the interference

patterns observed in the upstream region.   On

November 23, 1977, at 8^h 19^m 14^s ISEE-1 was located

in the upstream region at a radial distance of 19.8

R_E.   Starting at 8^h 19^m 14^s, the bottom of the inter-

ference pattern marked by a horizontal bar is at

about 4 KHz.   At 8^h 19^m 16^s, the bottom of the inter-

ference pattern has shifted downward about 500 Hz.

At 18.5^s the lower portion of the interference pat-

tern has dropped to about 3 kHz and one half space-

craft rotation later at 20.1^s it is down near 2 kHz.

The interference pattern retains its shape, but

shifts in frequency as the magnitude of the wave

vector or its direction with respect to the solar

wind changes.

A-G83-114

ISEE-1 WIDEBAND DATA

NOVEMBER 23, 1977 DAYS 327 ORBIT 13

R = 19.8 R$_E$ MAG LAT = 30.2°   MLT = 8.9 HRS
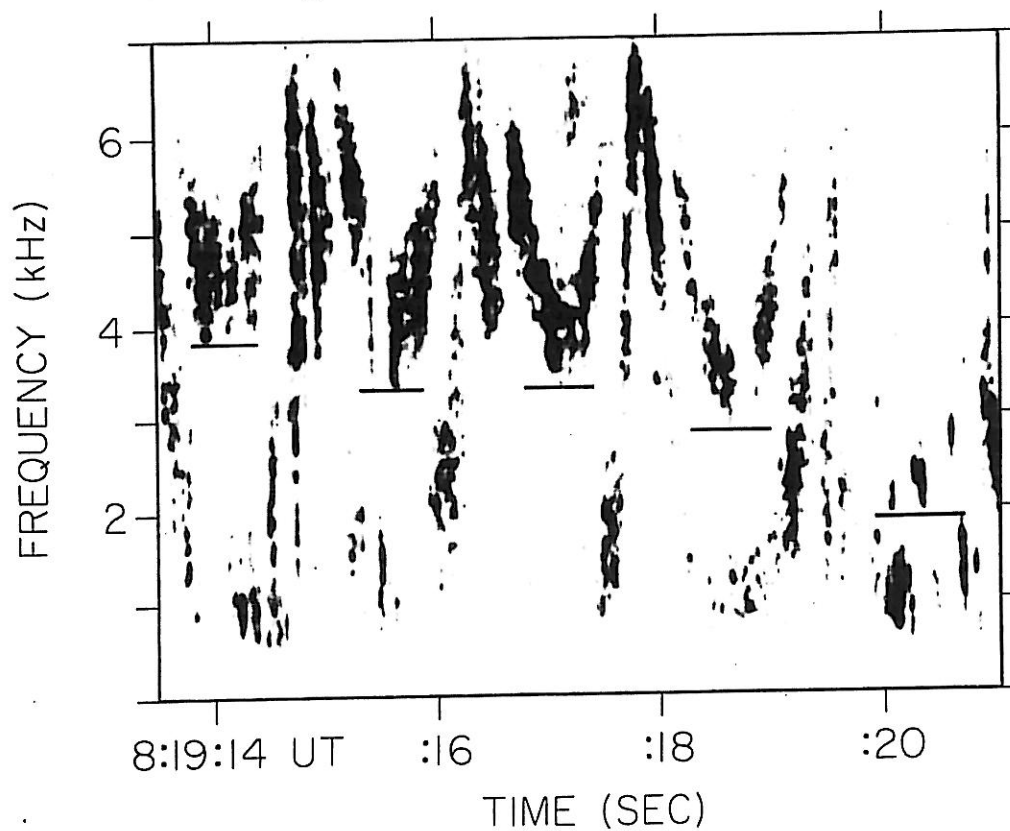

Figure 5

Figure 6   Wideband spectra for ISEE-1 at two different times on

day 326 are shown superimposed on an equatorial pro-

jection of the ISEE-1 orbit. At 6^h 56^m ISEE-1 is

located near the bowshock in the upstream region.

The ion waves are observed to have Doppler shifts of

up to 10 kHz. At this time the solar wind velocity

is about 300 km/sec and directed almost antisunward.

The spectrogram starting at 9^h 25^m 26^s was taken when

ISEE-1 was in the outer magnetosheath close to the

bowshock. The Doppler-shifted waves extend up to

about 4 kHz because at this time the plasma bulk flow

velocity is only about 160 km/sec, a little over half

that of the solar wind.
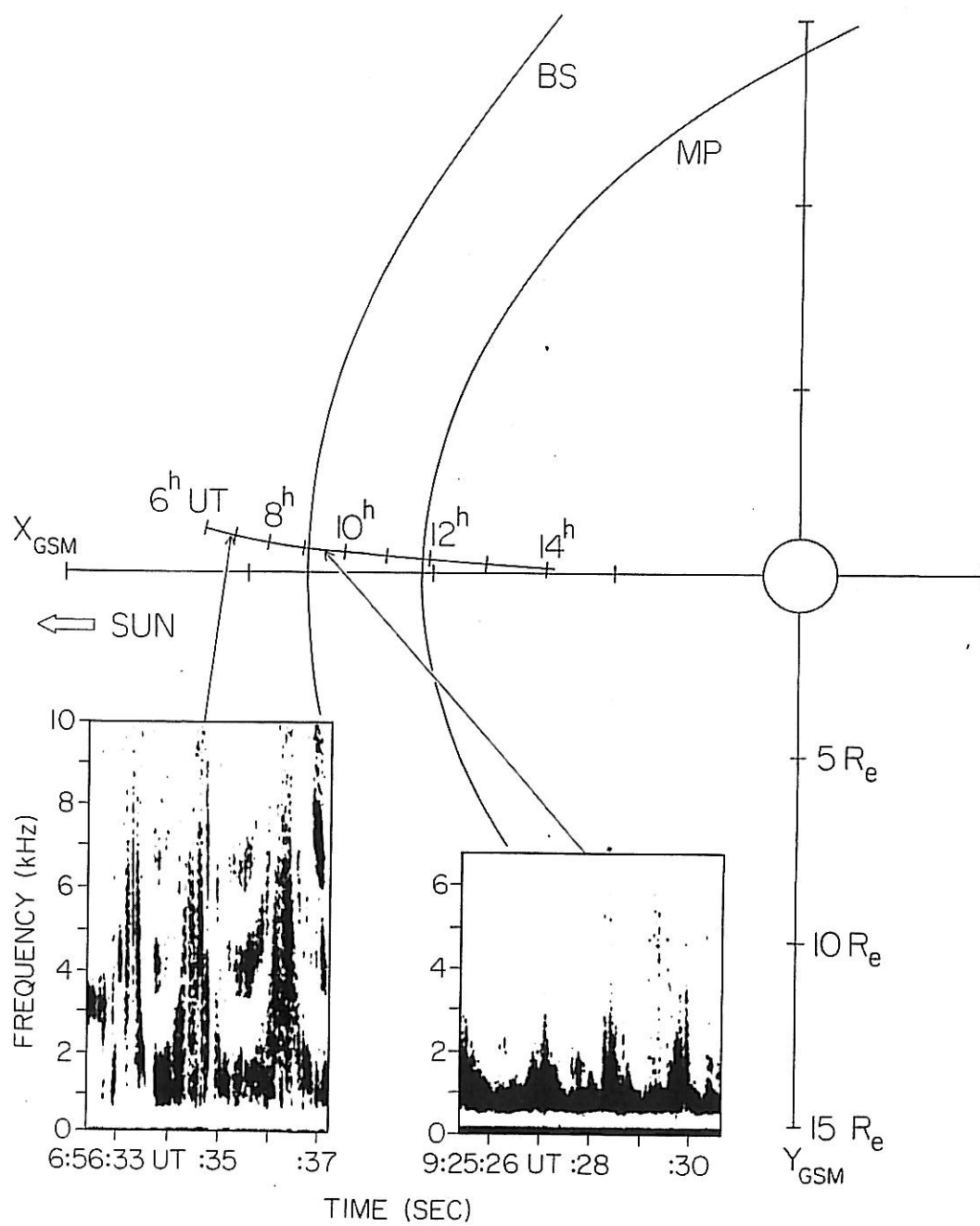
C-G82-318-1

EQUATORIAL PROJECTION OF ISEE-1 ORBIT
YEAR 1977 DAY 326

Figure 6

Figure 7   Illustration of the method of determining the spin

plane projected direction of propagation of the ion

waves when interference patterns are observed in the

wideband data. The time to in the wideband data in

the upper left hand corner corresponds to the spin

plane projected wave vector aligned along the space-

craft antenna. This antenna-x-axis direction can be

determined from the data tape for this time and the

direction can be compared to the spin plane projected
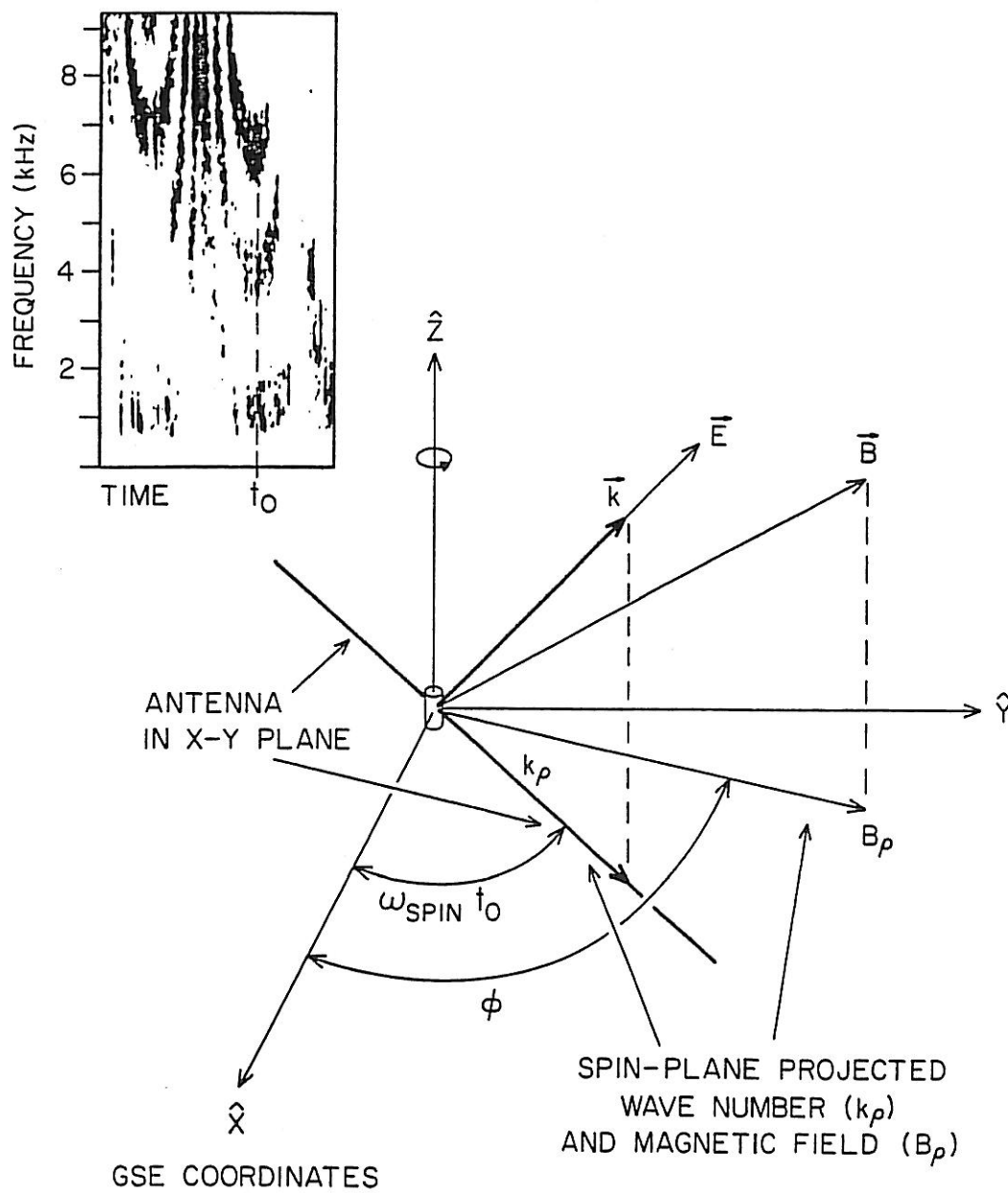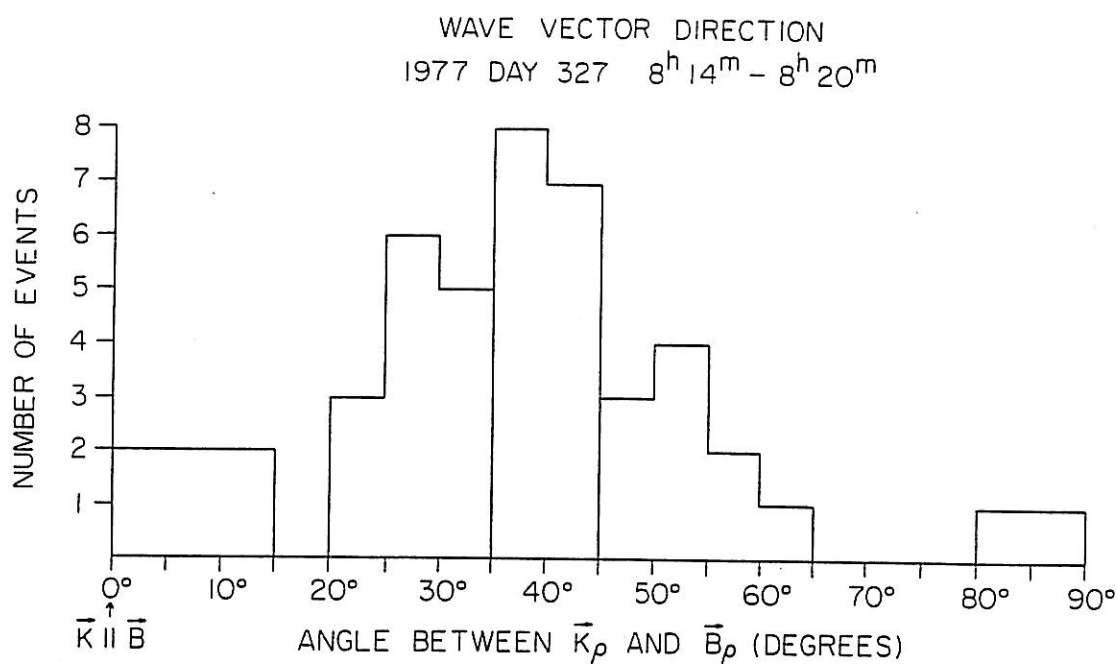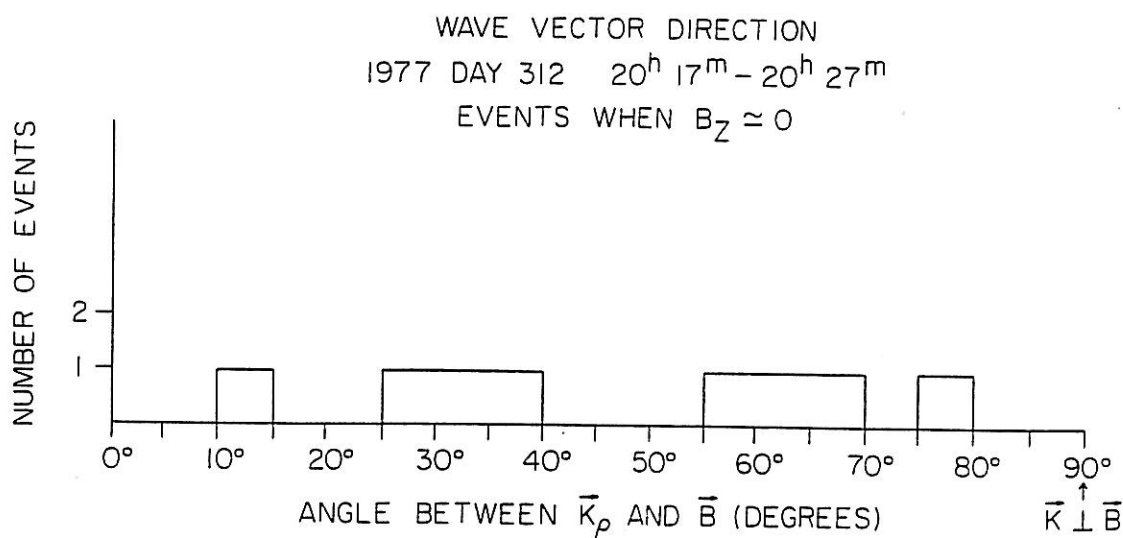
magnetic field.

A-G83-I65

Figure 7

Figure 8   Histograms of the observed angle between the spin

plane projected wave vector and the spin plane

projected magnetic field.

a) The upper panel is a histogram of the 47 separate

measurements of the angle between the spin plane

projected wave vector and the spin plane projected

magnetic field. If the wave vector were parallel to

the magnetic field then the angle between the

projected wave vector and the projected magnetic

field would always be zero. Because the angle is

rarely observed to be zero one can conclude that the

wave vector is not parallel to the magnetic field.

b) The lower panel shows 8 events observed on

November 8, 1977, from 20^h 12^m to 20^h 27^m when the z

component of the magnetic field was zero. If the

wave vector were perpendicular to the magnetic field

all events would have spin plane projected angle of

90 degrees. Because the angle is not observed to be

90 degrees, one can conclude that the wave vector is

not perpendicular to the magnetic field.

B-G83-284-1

WAVE VECTOR DIRECTION
1977 DAY 327 $8^h 14^m - 8^h 20^m$

a)

WAVE VECTOR DIRECTION
1977 DAY 312 $20^h 17^m - 20^h 27^m$
EVENTS WHEN $B_Z \simeq 0$

b)

Figure 8

Figure 9   An example of the geometry for a particular observed interference pattern on November 8, 1977, at 20^h 27^m 33.4^s. At this time ISEE-1 was located in the upstream region at about 17.1 R_E and 8.4 hours magnetic local time. The spacecraft z component of the magnetic field was very nearly zero for this particular event. The spin plane projected wave vector is 39 degrees from the magnetic field. If the wave vector were perpendicular to the magnetic field then the spacecraft z component of the wave vector would have to be extreemly large to account for the small projected angle relitive to the magnetic field. From this example and others like it one can assume that the wave vector is not perpendicular to the magnetic field.

A-G83-179

EVENT GEOMETRY FOR
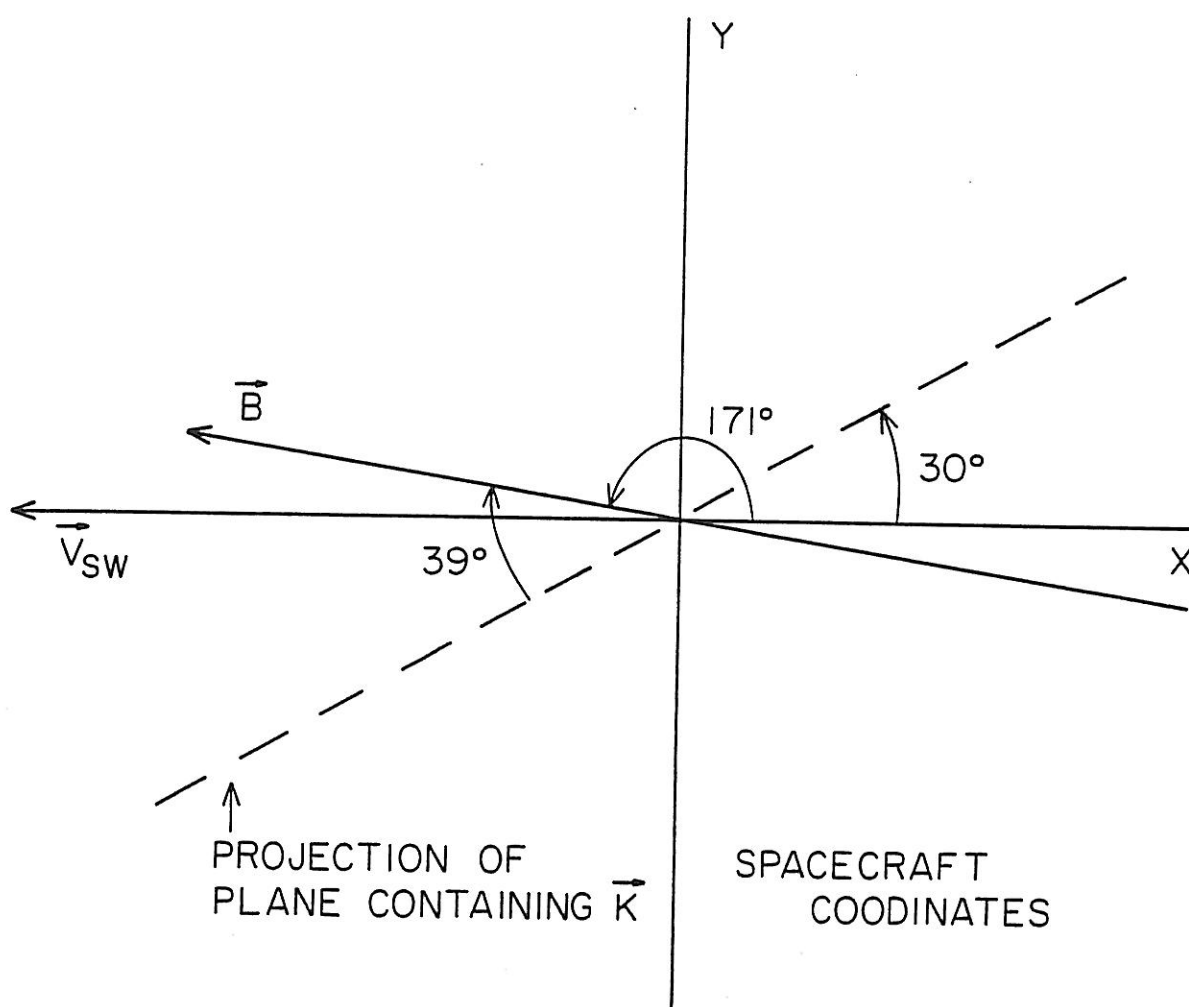## NOVEMBER 8, 1977 20^h 27^m $33.^s4$

Figure 9

Figure 10   Seven computer generated intensity versus frequency

plots centered around $6^h\ 44^m\ 17.9^s$. The event

illustrated in Figure 4 was reproduced by a total of

80 of these plots spaced at intervals of 50 milli-

seconds. These 80 computer generated plots were

used to determine the observed frequency and time of

a particular $k_{\rho Null}$ with less uncertainty than if

the wideband film were used. The two points identi-

fied at $6^h\ 44^m\ 17.9^s$ were used in the calculation of

the Doppler shift of the ion waves.

Figure 10

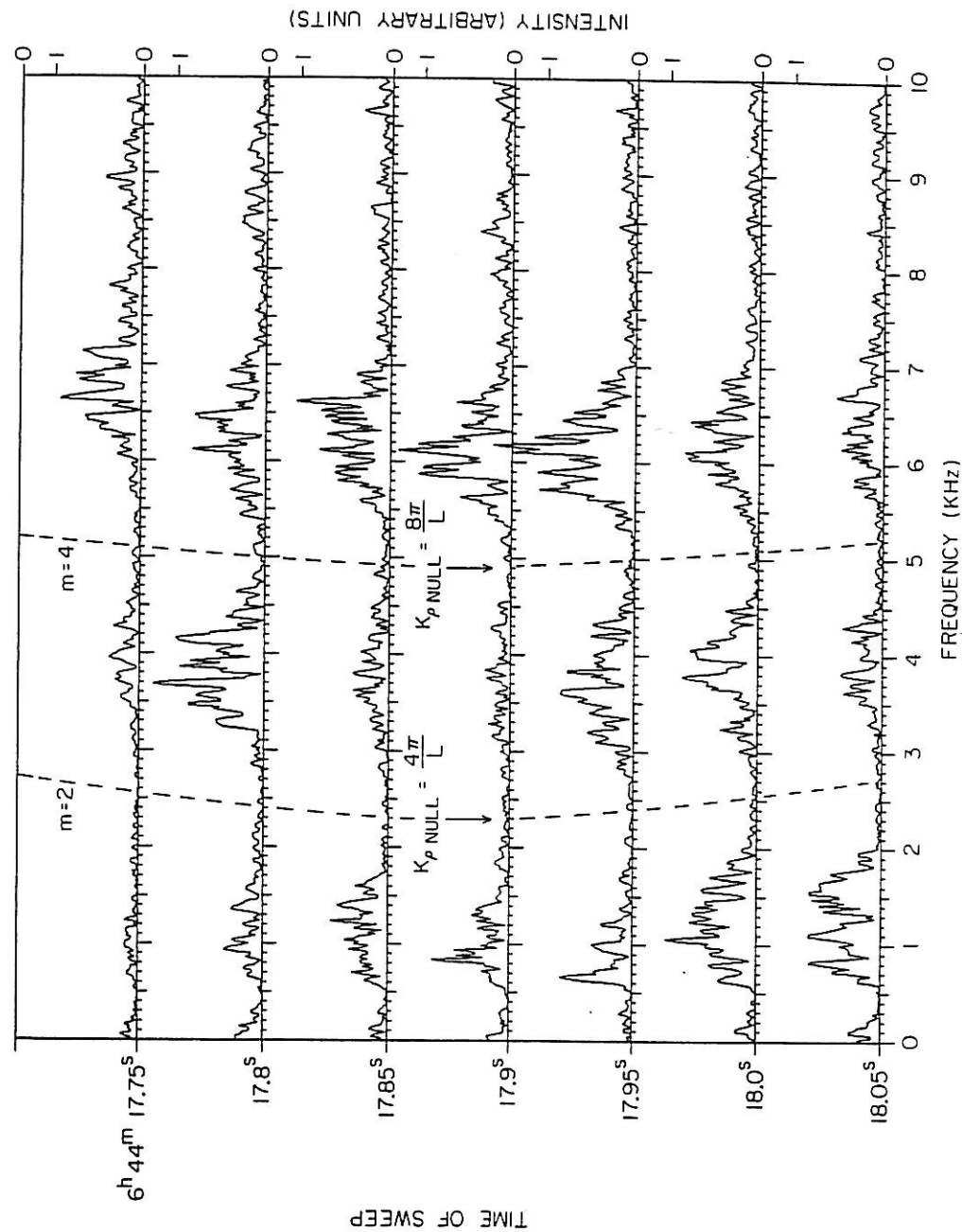ISEE - I   INTENSITY -vs- FREQUENCY
NOVEMBER 22, 1977
50 ms/SWEEP

C-G83-304-2

Figure 11   The geometry for the event in Figure 4. The spin

plane projected wave vector direction was determined

from the time of minimum in frequency in the wideband

data. The solar wind velocity and direction was

obtained from the solar wind instrument on ISEE-1 and

provided by W. C. Feldman.

A–G83–219

EVENT GEOMETRY
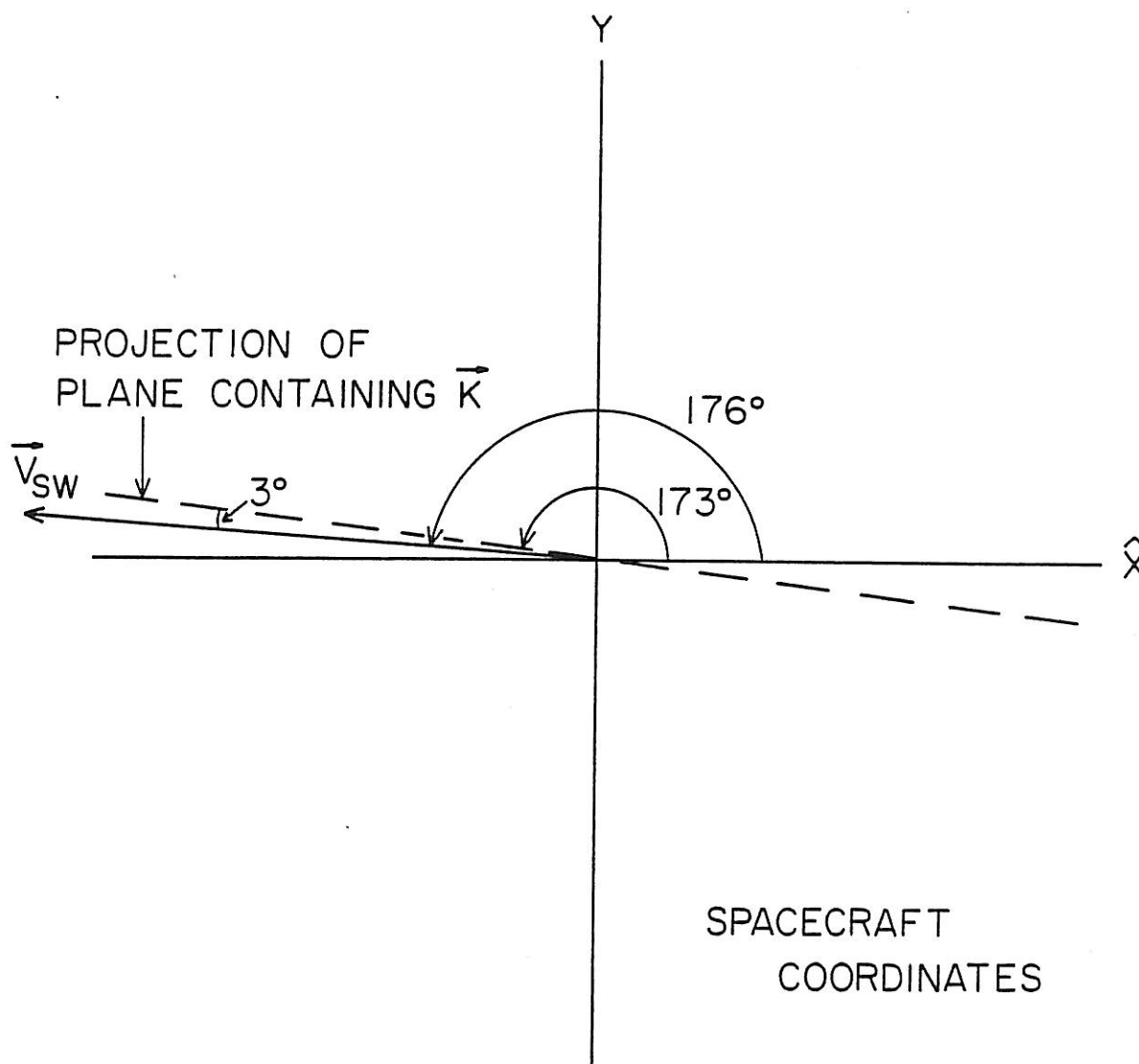FOR NOVEMBER 22, 1977 6^h 44^m $17.^s9$

Figure 11

Figure 12   The normalized dispersion curve of ion acoustic

waves with wave vectors that have propagation angles

of 75°, 60°, 30°, and 0° out of the spacecraft spin

plane are shown. The x-axis is the magnitude of the

spin plane projected wave vector normalized by the

Debye length. The y-axis is the rest frame fre-

quency normalized by the ion plasma frequency. The

data points on the graph are the points listed in

Table 1, normalized by the Debye length and the ion

plasma frequency. These normalization parameters

for November 22, 1977 are listed in Appendix B.

B-G83-233-1

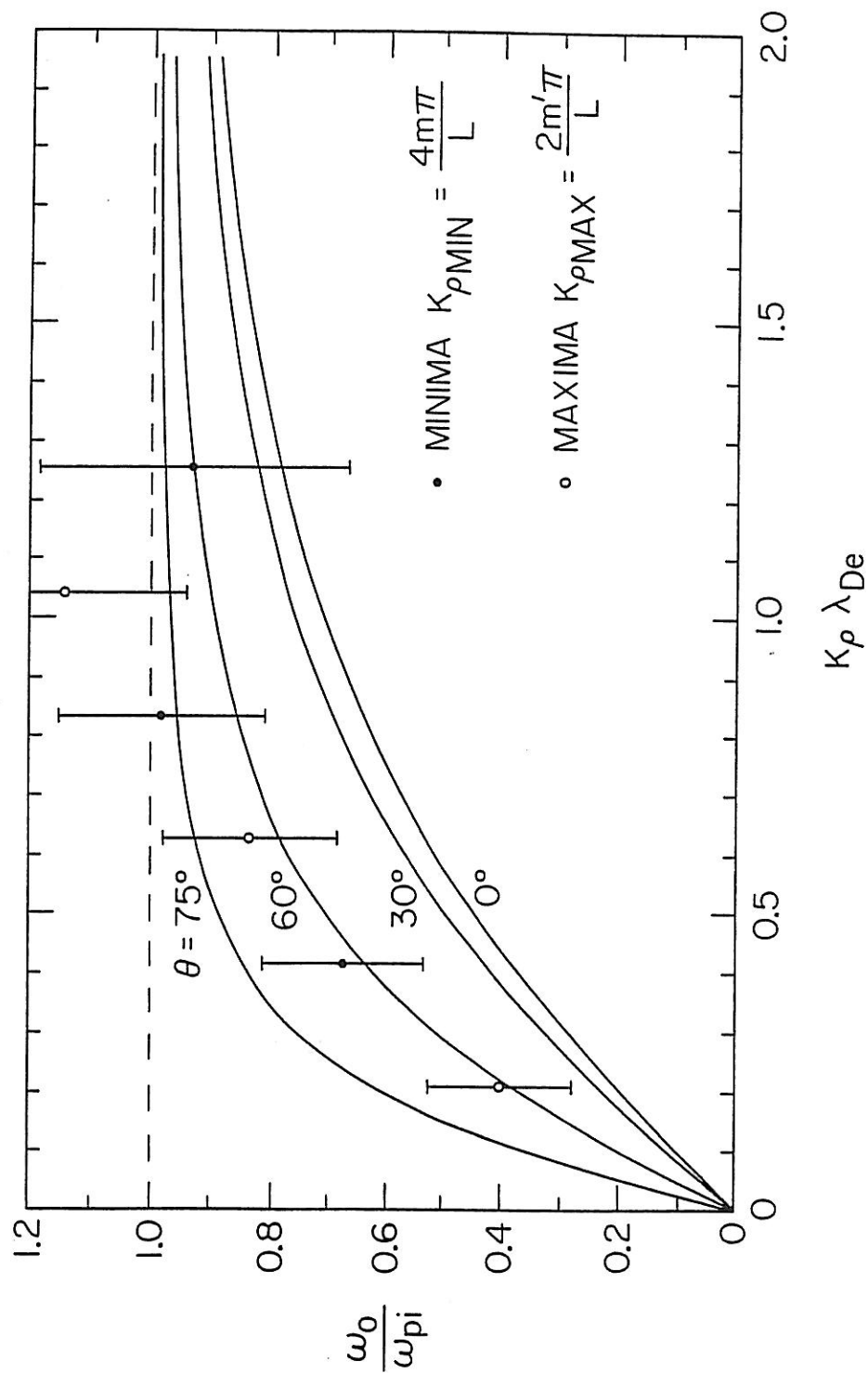NORMALIZED FREQUENCY VERSUS NORMALIZED WAVE NUMBER
FOR ION ACOUSTIC WAVES

- MINIMA $K_{\rho MIN} = \dfrac{4m\pi}{L}$

- MAXIMA $K_{\rho MAX} = \dfrac{2m'\pi}{L}$

$\theta = 75°$

$60°$

$30°$

$0°$

$\dfrac{\omega_o}{\omega_{pi}}$

$K_\rho \lambda_{De}$

Figure 12